Ocean Engineering 227 (2021) 108654

Contents lists available at ScienceDirect

Ocean Engineering

journal homepage: www.elsevier.com/locate/oceaneng

The power flow and the wave energy flux at an operational wave farm: Findings from Mutriku, Bay of Biscay

Gabriel Ibarra-Berastegi [a,b,*], Alain Ulazia [c], Jon Sáenz [b,d], Paula Serras [a], Santos J. González Rojí [e,f], Ganix Esnaola [g,b], Gregorio Iglesias [h,i]

[a] Department of Energy Engineering, University of the Basque Country (UPV/EHU), Bilbao Engineering School, Bilbao, Spain
[b] Plentzia Itsas Estazioa. PIE, University of the Basque Country (UPV/EHU), Plentzia, Spain
[c] Department of Energy Engineering, University of the Basque Country (UPV/EHU), Gipuzkoa Engineering School, Eibar, Spain
[d] Department of Physics, University of the Basque Country (UPV/EHU), Leioa, Spain
[e] Oeschger Centre for Climate Change Research, University of Bern, Bern, Switzerland
[f] Climate and Environmental Physics, University of Bern, Bern, Switzerland
[g] Department of Energy Engineering, University of the Basque Country (UPV/EHU), Gipuzkoa Engineering School, Donostia, Spain
[h] School of Engineering & Environmental Research Institute, University College Cork, Cork, Ireland
[i] School of Engineering, Computing and Mathematics, University of Plymouth, Drake Circus, Plymouth, PL4 8AA, United Kingdom

ARTICLE INFO

Keywords:
Mutriku wave farm
Self-organizing maps
Bay of Biscay
Wave climate
OWC
Fluid mechanics

ABSTRACT

Mutriku is a wave farm on the Spanish coast of the Bay of Biscay that has now been continuously supplying electricity for more than nine years. Since 1979, there has been a growing trend in wave energy flux for the whole Bay of Biscay. ERA5 data at the grid point nearest to Mutriku indicate an increase of 0.146 kW/m per decade for the 1979–2019 period. In this paper, a Self-Organizing Map (SOM) with a 2X5 architecture has been fitted to identify ten major sea-state types, each with a distinctive electricity generation pattern at a daily scale. This rendered it possible to reconstruct the daily electric power that would have been generated if the Mutriku wave farm had been operational over the entire 1979–2019 period and, accordingly, evaluate the impact that the observed changes in the wave climate and associated wave energy flux would have had on the electricity production. The results indicate that the electricity production or power flow would have remained constant during that period despite the increasing trend in wave energy flux. This is due to the regulation procedures and mechanisms used in the operation of Mutriku's Oscillating Water Column (OWC) wave energy converters, which dampen the effect of the increasing trend observed. The main conclusion is that the power flow levels off above a given threshold, making it more stable than the wave energy flux.

1. Introduction

The Mutriku wave farm is located on the Spanish coast of the Bay of Biscay (Fig. 1), an area long known for its wave energy po-tential (Iglesias and Carballo, 2010). This facility came into operation in 2011 (Pérez-Collazo et al., 2015). It is a breakwater-integrated wave farm consisting of 14 Oscillating Water Column (OWC) wave energy converters (Pereiras et al., 2015; López et al., 2016; Zheng et al., 2019; Zheng et al., 2020a; Zheng et al., 2020b).

Mutriku is the only wave farm in the world continuously supplying electricity to the grid (O'Hagan et al., 2016) and its major operational aspects have been reported in this journal by the authors (Ibarra-Berastegi et al., 2018; Serras et al., 2019).

Previous studies for the area indicate that the energy carried by waves has been increasing in the Bay of Biscay since 1900 (Ulazia et al., 2017). The effect that WEF increasing trends have on the electric output of the different types of wave energy converters (WEC) is yet to be studied in detail. Much of the literature on wave energy has used the standardized wave energy transport flux. However, the power flow from a wave farm is clearly quite different from the flux. The wave energy flux increases as a function of the squared wave height and the period. In most WEC converters, the power initially rises as a function of the period, and then levels off as the period increases. As a result, the power flow is much more stable (Antonio, 2010; Reikard et al., 2015). In the particular case of Oyster-type WECs (Antonio, 2010), some works for the same area suggest (Folley et al., 2007; Ulazia et al., 2019) that the WEC's

* Corresponding author. Department of Energy Engineering, University of the Basque Country (UPV/EHU), Bilbao Engineering School, Bilbao, Spain.
E-mail address: gabriel.ibarra@ehu.eus (G. Ibarra-Berastegi).

https://doi.org/10.1016/j.oceaneng.2021.108654
Received 1 October 2020; Received in revised form 18 January 2021; Accepted 18 January 2021
Available online 6 April 2021

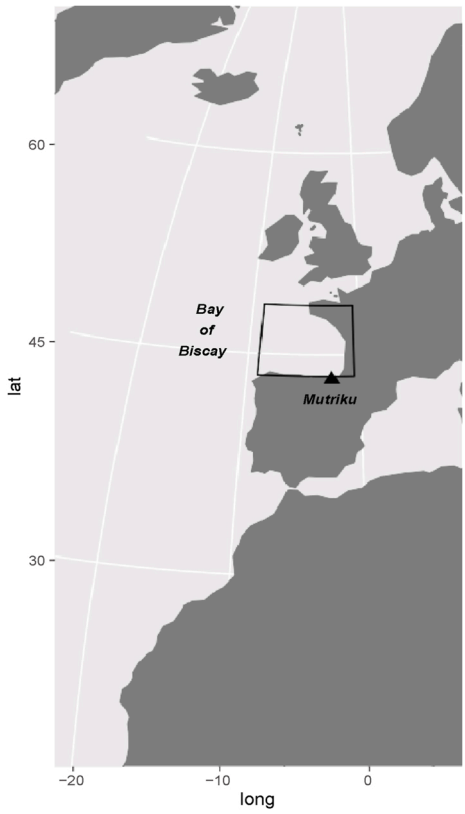

Fig. 1. Mutriku wave farm is located in the Bay of Biscay.

efficiency at transforming wave energy into electric power would be reduced. In these studies, the trends were calculated by combining ERA-Interim and ERA-20C reanalyses (ECMWF, 2020) to extend the calculation period back to 1900. Now, the Bay of Biscay's wave climate trends corresponding to the 1979–2019 period have been calculated here using homogeneous monthly data from the more recent ERA5 reanalysis alone (Hersbach, 2016).

The impact these wave energy trends have on the electric power generated at a fully operational wave farm like Mutriku, will be analysed here for the same period. However, this wave farm only came into operation in 2011 and operational data have only been intermittently available since then. Learning how Mutriku and wave climate relate using the few common years of the whole 1979–2019 period, can therefore be used to estimate the power generated throughout the entire period. The idea is that if some common years are available with both types of data (i. wave data, ii. electric yield from Mutriku) it is possible to learn and mathematically describe how the energy transfer takes place from waves (input, hydraulic energy) to wire (output, electric power). This mathematical description, if accurate, can be used to estimate the electricity generated in Mutriku for the years in which only wave data (input) are available. This can reveal the impact of wave climate trends in the Bay of Biscay on the power generated at the Mutriku wave farm.

The objectives of this paper are as follows:

1. To calculate the wave climate trends in the Bay of Biscay over the 1979–2019 period.
2. To design a data-driven statistical model to relate wave energy in the area and electric power generation at the Mutriku wave farm.
3. To reconstruct the power generation series at Mutriku for the 1979–2019 period using this model applied to the historical ERA5 wave energy records.
4. To evaluate the impact that wave climate trends have on the electric power trends at Mutriku for the 1979–2019 period.

The paper is structured as follows: the next section describes the data used and the research methodology. The results are then presented in Section 3. Section 4 discusses the results and the final section provides the conclusions and future outlook.

2. Data and methodology

2.1. Data

Two different data sources have been used for this study. On the one hand, ERA5 wave hourly data for the 1979–2019 period have been downloaded from the Copernicus Climate Data Store Copernicus Climate Data Store (2020). ERA5 provides a spatial resolution of 0.5° for oceanic variables. The geographical boundaries here cover the Bay of Biscay and include 176 grid points, with 16 positions in longitude [-9° E, −1.5° E] and 11 in latitude [43.5° N, 48.5° N]. For this study, the following variables from the ERA5 reanalysis have been downloaded:

1. Significant wave height H_s
2. Mean wave direction m_{wd}
3. Energy mean wave period T_m
4. Wave peak period T_p

The wave energy flux (*WEF*) per unit of wave-crest length in deep waters, with units of kW/m, has been calculated (Bidlot, 2020; Multon, 2013) as follows:

$$WEF = 0.49 \cdot T_m H^2 \quad (1)$$

WEF is a vectorial magnitude and its zonal WEF_u and meridional WEF_v components were derived by combining *WEF* and the mean wave direction m_{wd}.

The operational data used have been retrieved from the Supervisory Control and Data Acquisition (SCADA) at the Mutriku wave farm which is run by the Basque Regional Government through the Biscay Marine Energy Platform (2020). Hourly data from 2014 to 2016 were disclosed in 2017 and used to characterise this farm's most relevant aspects (Ibarra-Berastegi et al., 2018; Serras et al., 2019). A new dataset belonging to the August 2018–July 2019 period has recently been released by the Basque Energy Agency (2020). This dataset includes records of the power generated by the facility's second turbine (T02) taken by SCADA with a sampling interval of 0.5 s.

Following our previous works (Ibarra-Berastegi et al., 2018; Serras et al., 2019), the average electric power (in kW) generated by T02 over the preceding 5 min at hourly time steps, (each calculated on 2X60X5 = 600 SCADA instantaneous power records) has been adopted as the reference variable and it will be referred to here simply as the electric power. Daily averages of the electric power generated by T02 corresponding to both periods have been used and this variable will be denoted as T02pow.

2.2. Methodology

This paper's first objective was to calculate the wave climate trends for the Bay of Biscay, so 492 monthly WEF averages were computed for the 1979–2019 period at the 176 grid points in the area and trends were calculated on their anomalies by subtracting their seasonal cycle. A Theil-Sen robust estimation of trends was carried out (Siegel, 1982; Sen, 1968; Theil, 1950) and their significance was assessed at a 95% confidence level. The second objective involved building a data-driven statistical model to relate waves and electric power generated by Mutriku's T02 turbine. At this initial stage, to that purpose, it was decided that two

major types of statistical models needed to be tested. On the one hand, a non-linear regression approach with different types of algorithms. On the other hand, several classes of classification techniques. In all cases, the candidate models needed to be built on a training dataset and their performance assessed on an independent test dataset.

At this point, it is important to note that the electricity generated at the Mutriku wave farm exhibits a clear seasonality (Ibarra-Berastegi et al., 2018) with significantly higher values in winter than in summer. However, at the preliminary stages of this study the simple replication of the seasonal cycle observed at the training stage could not successfully represent the monthly, seasonal and annual ob-servations of the test dataset. This implied that a specific model was needed to override the seasonal cycle.

This research used hourly values from ERA5 wave data at Mutriku's nearest grid point [-2.5° E, 43.5° N] and 3262 hourly power records corresponding to the 2014–2016 period were used to fit the candidate models. This was the training database. The test dataset was constituted by 8760 records of the same variables corresponding to the August 2018–July 2019 period. The performance of all the candidate models was evaluated on these test cases reserved from the beginning for this purpose.

The general aim was to analyse the impact of wave climate trends on the electric power at Mutriku. The time scale for the wave trends was monthly, so the model should also be able to successfully reproduce the observed monthly averages of the electric power generated at Mutriku corresponding to the test dataset. Additionally, the model should also accurately capture seasonal and annual averages. Using generally accepted criteria (Camus et al., 2019; Reguero et al., 2015) the year was divided into the Northern Hemisphere four seasons: winter, (WI) running from December to February (DJF); spring (SP), from March to May (MAM); summer (SU) from June to August (JJA) and autumn (AU) from September to November (SON). For the three time scales (monthly, seasonal and yearly) the null hypothesis should be satisfied; that is, the differences between observations and model predictions on the test dataset should not be different from 0 at a 95% confidence level. These confidence intervals were estimated using bootstrap resampling.

A regression approach was initially used to build a model that could mathematically relate the waves observed near the Mutriku wave farm and the electricity produced. Wave data belong to the nearest ERA5 grid point [-2.5° E, 43.5° N] to Mutriku (~22 km). Regardless the specific algorithm employed, under this regression scheme, the inputs would be the wave data and the output the electric power at Mutriku. Random forest is a machine-learning type regression algorithm that is good at capturing non-linear relationships between a set of inputs and outputs. Due to the authors' experience (Serras et al., 2019; Ibarra-Berastegi et al., 2015, 2016) using this type of algorithm and the nonlinearities that could be expected to be present, an initial attempt to use random forest applied to daily data was made. This approach proved unsuccessful at reproducing turbine T02's observed monthly, seasonal and annual power averages for the test period.

This prompted an alternative approach based on a classification scheme for identifying a number of sea-state types. When Mutriku was designed, lab-scale tests were also carried out for a certain number of sea-states using the limited information available at that time (Torre-Enciso et al., 2009). Certain classification techniques like simulated annealing or k-means have already been used to identify sea-state types for the entire Bay of Biscay (Le Cozannet et al., 2011; Abadie et al., 2006; Butel et al., 2002), extended areas (Camus et al., 2014; Perez et al., 2015) and at global level (Fairley et al., 2020). Large-scale wave climate studies have also used principal components analysis to identify sea-states at a global level (Camus et al., 2019).

The field of study here covers a small area of the Bay of Biscay near Mutriku, and Self-Organizing Maps (SOMs) have been adopted as a classification tool. SOMs are a type of neural network intended for classification purposes that have been widely used in geophysical applications (Gibson et al., 2017; Vilibic et al., 2016; Ezcurra et al., 2008; Ibarra-Berastegi et al., 2009).

More specifically, SOMs have been used in oceanography to identify sea-state types (Camus et al., 2011; Liu et al., 2006), including extreme wave climate patterns (Barbariol et al., 2016). SOMs can operate either in supervised or unsupervised mode. In the former case, a classification of (at least some) cases is known beforehand and these cases are presented to the SOM, which is fitted to capture the underlying classification rules. In the latter, unsupervised mode, classification examples are not available and cases are mapped onto the different nodes by preserving nearness. Starting from random initial values, SOM parameters are fitted using a competitive learning algorithm that preserves the topological properties of the input space. Once fitted, the SOM will be able to classify new cases presented to it. Details of the more mathematical aspects of this type of neural networks can be found in the literature (Kohonen, 1982; Kohonen, 1991; Kohonen, 1997; Kohonen and Somervuo, 2002; Wehrens Buydenset al., 2007).

SOMs have been applied here to:

1. Identify the most relevant sea-state types for the area around Mutriku.
2. Classify each day by sea-state types using wave data.

SOMs can also be understood as a technique that projects or *maps* a set of cases defined in a multidimensional space onto a regular 2D grid while maximizing the preservation of their original distances. In other words, those cases close to each other in the original hyperspace (similar sea-states in our study) will also cluster together in the different nodes of the 2D lattice. The projected 2D grid has a limited number of nodes which in our case represent sea-states obtained as the combination of all the similar types projected onto the same node. All the observed daily sea-states can therefore be grouped into a reduced number of sea-state types or nodes on the SOM (see Appendix A for further details).

Additionally, each node or sea-state type belonging to every candidate SOM, has been assigned a characteristic daily value for the electric power generated by Mutriku's second turbine. This value is denoted in this paper as T02pow. It has been calculated as the median of the daily average power generated by T02 in the days belonging to a particular sea-state type in the training database.

Once a SOM has been fitted with the training data, it can classify a sequence of new daily sea-states presented to it as belonging to one of the logged sea-state types. Since a characteristic value of the electric power (T02pow) has already been assigned to each sea-state type, a series of daily power values generated by T02 can be easily derived from the classification provided by the SOM.

We did not have any data on the layout and number of nodes (or sea-state types) of the optimal SOM and the algebraic definition of the original hyperspace based on wave variables so a large number of candidate SOM networks needed to be fitted in unsupervised mode. All these candidate networks would have a different number of sea-state types (nodes) and associated T02pow values. A wave farm like Mutriku is a facility that converts hydraulic energy from waves into electric power. The candidate oceanic variables were therefore those that concentrate the directional information on wave energy (WEF_u and WEF_v) and the frequency associated with the maximum energy (T_p).

The appropriate SOM here would be one in which the sequence of T02pow values derived from the test dataset's classification by sea-state types could successfully predict the monthly, seasonal and yearly means. The number of nodes would also represent the optimal division of wave data into the representative sea-state types needed to accurately describe the power generated. This approach is different from previous

works in which SOMs have been applied to identify sea-states characterized by the wave energy flux (Barbariol et al., 2016).

To identify this optimal SOM, an iterative process was designed in which more than 1000 SOMs with different architectures were fitted on the training dataset. This also involved evaluating a number of different options to correctly select the input wave variables that constitute the hyperspace in which each daily sea-state is defined.

The first stage of this iterative process, involved fitting each candidate SOM on the training dataset, allowing a maximum of 10,000 iterations. The SOM obtained was then used to classify the test dataset's wave data by daily sea-state types. This classification used the assigned power values for each sea-state type to easily derive a time series of daily electric power averages for T02. The last stage involved evaluating the capability of the daily power predictions obtained in this way to reproduce the T02's electric power at monthly, seasonal and yearly scales. The means observed and predicted for these timeframes were compared at a 95% confidence level using bootstrap resampling.

The result of these iterations led to the definition of each daily sea-state in an 18-dimension hyperspace constituted by the standardized ERA5 values at the nearest grid point every 4 h corresponding to WEF_u, WEF_v and T_p. That is, on a given day, the hourly values of the zonal and meridional wave energy flux and the peak wave period at 00 h-04 h-08 h-12 h-16 h–20 h constitute an 18-dimensional hyperspace and that particular day's sea-state appears as a point on it.

The optimal SOM had 10 nodes displayed in a 2X5 lattice. This SOM was used to build the series of daily power values obtained from the daily sequence of sea-state types. The daily values of T02pow predicted in this way were compared to the 365 observations of the test data set, yielding a determination coefficient (R^2) of 0.72, a RMSE value of 1.51 and a mean absolute error of 1.01 kW. However, as mentioned above, the time scale of interest on which results needed to be evaluated was monthly, not daily. This daily time series was used to compute monthly and seasonal averages for the test data set and compared to observations using 95% confidence level intervals obtained by bootstrap resampling.

Fig. 2 shows that the final SOM obtained successfully reproduced all the monthly and seasonal averages. In all cases, the confidence intervals of ob-servations and predictions overlap, thus confirming that at a 95% confidence level, the null hypothesis of equal values for predictions and observations is attained. The same can be concluded about the 95% confidence interval of the yearly average T02pow observations (2.2–2.8 kW) and predictions (2.1–2.7 kW). It is important to stress that this particular combination of 18 dimensions and a 2X5 grid was the only one among all the candidates tested to successfully predict all the power averages in the test dataset at monthly, seasonal and yearly time scales.

To meet the third objective, this SOM was used to classify the sea-states for all the days corresponding to the 1979–2019 period. This sequence of daily sea-states was used to estimate, the 14,975 daily T02pow values generated by T02 at Mutriku for the same period. Finally, to comply with the fourth objective, the trends in monthly power values for the 1979–2019 period were computed to evaluate the impact that wave energy changes in the Bay of Biscay have on the electric power generation at Mutriku. This included calculating trends in the frequency of occurrence and in the average distance to ideal sea-state types. In all cases, robust Theil-Sen trends were calculated and their significance was assessed at a 95% confidence level.

3. Results

3.1. WEF trends in the Bay of Biscay

Fig. 3 shows the Theil-Sen trends in the wave energy flux in the Bay of Biscay in kW/m per decade. They are significant at all the grid points at a 95% confidence level. There are positive trends in the whole area for the 1979–2019 period, albeit with a significant spatial gradient. The trends record a value of around 0.1 kW/m per decade in the innermost parts of the Bay of Biscay, with average values below 15 kW/m. More specifically, the observed trend at the ERA5 pixel including Mutriku (centered at −2.5° E, 43.5° N) is 0.14 kW/m per decade, with an average *WEF* value of 13.9 kW/m. As we move out into open sea, the positive trend strengthens to a maximum of 1.8 kW/m per decade in areas where the average values of *WEF* are below 40 kW/m.

These values are consistent with previous studies for *WEF*, H_s and T_m (Ulazia et al., 2017; Le Cozannet et al., 2011; Abadie et al., 2006; Charles et al., 2012), which also indicate that wave heights and the wave energy

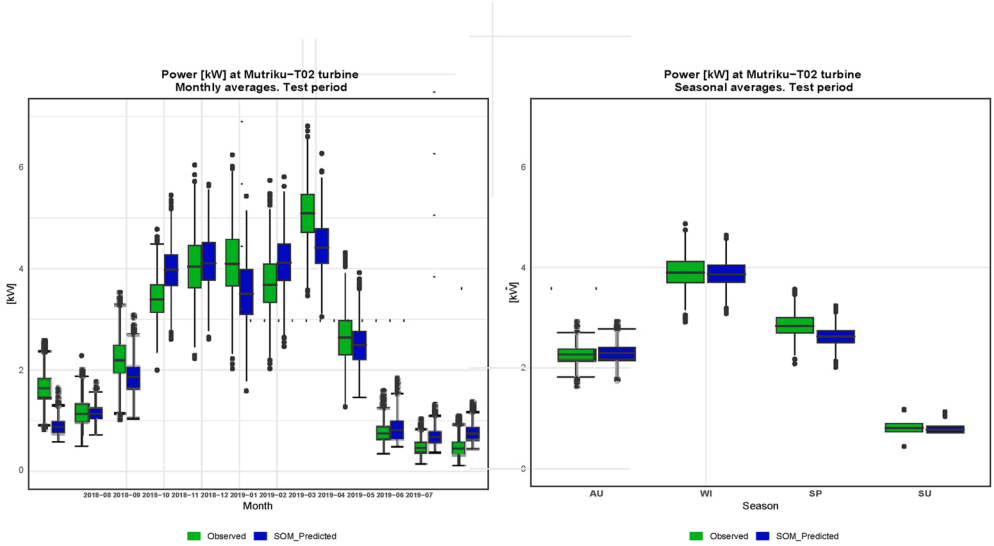

(a) (b)

Fig. 2. 95% confidence intervals of the observed and predicted electric power generated by T02 at Mutriku. Test period August 2018–July 2019. a) Monthly. b) Seasonal.

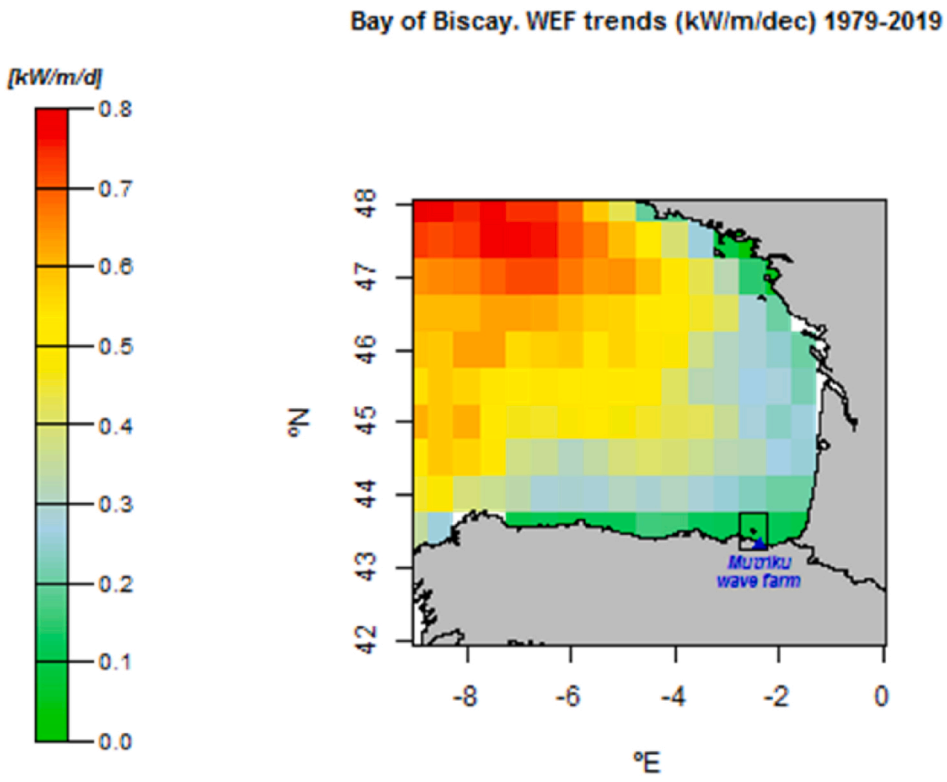

Fig. 3. *WEF* trends in the Bay of Biscay per decade (1979–2019) and ERA5 nearest grid point from Mutriku.

Table 1
Sea-state types and characteristic values for the 2 × 5 SOM.

Node/Sea-state type	H_s [m]	T_m [s]	*WEF* [kW/m]	T_p [s]	*WS* [m/s]	T02pow	Frequency [%]	Autumn [%]	Winter [%]	Spring [%]	Summer [%]
1	4.8	12.0	142.3	15.1	11.4	7.81	0.6	12.6	68.9	18.5	0.0
2	3.7	10.5	78.9	13.2	10.2	8.10	1.1	18.4	61.0	20.6	0.0
3	2.1	8.9	20.8	11.1	6.2	5.22	8.4	32.9	28.0	26.4	12.8
4	3.6	11.6	75.4	14.4	8.1	9.04	2.3	21.7	57.1	21.2	0.0
5	2.0	11.3	22.4	14.1	4.4	5.12	10.5	24.3	49.6	22.7	3.4
6	2.8	11.1	43.8	13.7	6.6	7.84	6.2	25.3	51.7	20.7	2.4
7	1.0	6.5	4.1	8.9	4.2	0.24	4.8	24.9	15.4	27.1	32.6
8	1.2	9.3	7.6	12.4	3.7	1.50	24.1	29.6	30.5	28.9	11.1
9	1.0	7.4	4.2	9.8	3.4	0.76	26.8	22.9	6.7	24.6	45.8
10	1.0	5.6	3.5	6.7	4.7	0.32	15.3	18.6	9.4	23.5	48.5

flux in the Bay of Biscay have been increasing in recent decades.

3.2. Sea-state types. Characterization and trends

As mentioned above, these trends have been correlated with the electricity generated at Mutriku through a classification approach and accordingly, an optimal SOM with a 2X5 architecture was finally fitted.

Table 2
Averages and decadal trends. ERA5 point (−2.5°E, 43.5°N), for 1979–2019.

Variable	Average	Trends units/decade
WEF [kW/m]	13.9	0.146
WEF_u [kW/m]	10.4	–
WEF_v [kW/m]	−8.1	−0.105
H_s [m]	1.47	0.012
T_m [s]	8.47	0.090
T_p [s]	10.87	0.064
T02pow [kW]	2.4	–
Sea-state type #3 frequency [%]	8.4	0.333
Sea-state type #7 frequency [%]	4.8	0.268
Sea-state type #9 frequency [%]	26.8	−0.284

Each of the 10 nodes represents a sea-state type at a daily scale obtained in the training dataset.

The sea-states are defined for the area near Mutriku as they provide the best information for the waves that reach it. Table 1 provides a summary of the characteristic values corresponding to the different sea-state types (nodes). It includes data on wind and waves as well as the representative T02pow associated with each sea-state type. The incoming direction of waves in all sea-state types is NW-NNW. The first two types correspond to highly or extreme sea-states with a low occurrence and average values that are substantially different to all the rest. A more visual representation of the final SOM's main characteristics and its associated sea-state types can be seen in Appendix B.

Table 1 also features each sea-state's frequency of occurrence and distribution by seasons. In the case of wind, the incoming direction is SSW for type #5 and SSE for sea-state type #8. For all the other types, the prevailing wind directions are W-NW. The waves at the nearest grid point to Mutriku record a small but significant positive trend, as can be seen in Table 2. In the case of *WEF*, the meridional component WEF_v accounts for this trend, thus indicating a shift northwards in the incoming wave direction. The significant wave height, mean wave

period and peak wave period also exhibit small but significant positive trends.

The wave energy flux, *WEF*, records significant positive trends for the 1979–2019 period as calculated from monthly means. This evolution could be explained (Le Cozannet et al., 2011) either by an increase of the *WEF* average of certain sea-state types or/and by a change in the relative frequency of occurrence of certain sea-state types. In this study, the evolution of the sea-state types obtained have been analysed also from these two points of view.

1. Changes within the 10 sea-state types as defined in the training period were detected by calculating trends in the distance of cases to the ideal 2X5 SOM for the whole 1979–2019 period. Additionally, trends were calculated for *WEF* values within each node. The results show that both distance and *WEF* trends within each sea-state type are not significant, thus indicating that they remain constant for the whole period.
2. Trends in the frequency of occurrence for the different sea-state types have also been calculated. Only in three sea-state types were significant changes detected, with a positive increase of 0.33 and 0.25% per decade in the frequency of occurrence of sea-state types #3 and #7 during the 1979–2019 period. Type #9 records a negative trend in frequency of −0.28%/decade (Table 2).

The conclusion is that the small increase in the frequency of a highly energetic sea-state type like #3 along with the decrease of #9 accounts in the area around Mutriku for the upward trend found in the monthly values of *WEF* during the 1979–2019 period.

3.3. T02pow monthly trends for 1979–2019

ERA5 data at the nearest grid point were used to classify the final 2X5 SOM for all the days corresponding to the 1979–2019 period by sea-state types. The daily time series of T02pow for the 1979–2019 was reconstructed by assigning the T02pow value in Table 1 derived from the training data set to each sea-state type. The monthly averages for T02pow and *WEF* for the whole period were 2.4 kW and 13.9 kW/m respectively. Table 1 shows that the sea-state types #1 to #6 correspond to above-average *WEF* and T02pow values. These more energetic types represent 29% of the cases and some of them, such as #1, #2, #4 and #6, mainly occur in winter. Types from #7 to #10 record characteristic below-average values of *WEF* and T02pow and account for 71% of the cases.

The trend in the daily time series of T02pow for the 1979–2019 period was also calculated. Due to its marked seasonality, this trend was calculated both on anomalies and original data, and in both cases was non-significant at a 95% confidence level (Table 2).

4. Discussion

Self-organizing maps have been used here to classify the waves observed near Mutriku into ten sea-state types using a 2X5 SOM. Prior studies (Le Cozannet et al., 2011; Abadie et al., 2006; Butel et al., 2002; Charles et al., 2012) have used different classification algorithms applied to broader areas of the Bay of Biscay to divide the observed waves into twelve major sea-state types.

Although prior studies have used other databases, following a completely different methodological approach and with a purely oceanic and not energetic focus, they also report an increase in wave energy and a shift northwards in the incoming direction. Similarly, the sea-state types are reported to remain constant and changes are attributed to the evolution in their frequency of occurrence. These important features were also apparent in our results, which confirms that they are key aspects for showing how wave energy potential has evolved in the Bay of Biscay in recent decades.

Our classification approach here made it possible to estimate the evolution of the wave energy flux during the 1979–2019 period and the electric power that would have been generated by the second turbine in Mutriku over the same period. The joint analysis of the evolution of both variables for that period indicates that the small changes detected in the wave trends near Mutriku have not involved significant changes in the electricity production.

This result can be explained by two factors:

1. The rather small trends in waves for the period 1979–2019 have been calculated at the nearest ERA5 grid point, 22 km off the Mutriku wave farm. Mutriku is a breakwater wave farm located on the shoreline, and probably, as can be deduced from the general behaviour of waves in the Bay of Biscay (Fig. 3), the trends in the waves actually reaching Mutriku's air chambers are even less marked.
2. The regulation and control of the Wells turbines in Mutriku are based on different adaptive models based on the instantaneous values of each generator's torque as input variable, and have been amply reported in the literature (Faÿ et al., 2020a; Amundarain et al., 2012; Amundarain et al., 2010; Lekube et al., 2018a; Lekube et al., 2018b). A secondary regulatory element includes a butterfly valve located in the duct connecting the air chamber and the Wells turbine. Depending on the energy of the incoming waves and in order to regulate the incoming flow from the air chamber, this butterfly valve may close totally or partially but its response is not instantaneous (see Appendix C).

Although turbine control is implemented instantaneously, a graphical representation of the *WEF* and T02pow on the same daily scale used here can describe how the regulation system acts to dampen the energy from incoming waves. Fig. 4(a) shows that as the *WEF* increases to 45 kW/m, the generated power increases linearly to a peak value of around 8.5 kW. *WEF* values above 45 kW/m do not lead to T02pow above values 8.5 kW, as the regulation mechanisms tend to dampen the increase in wave energy flux. The sea-state types obtained in this study are also aligned according to this general behaviour (see Fig. 4(b)).

Table 1 shows that the changes in *WEF* are concentrated in three sea-state types: #3, #7 and #9. Positive trends in sea-state type #3 and negative trends in #9 increase the wave energy flux. Positive trends in the occurrence of sea-state type #7 reduce the average wave energy flux. The combined trends for the 1979–2019 period have meant a positive trend of 0.146 kW/m per decade for *WEF* and no trend for T02pow.

Other effects gathered in the literature such as the sea-level rise at regional (Caballero et al., 2008; González et al., 2013) and global scale (Kulp and Strauss, 2019) do not seem to have any impact on Mutriku's electricity production.

In order to estimate the conditions conducive to changes in the electric power generated, a number of synthetic time-series for the 1979–2019 period were built increasing/decreasing the decadal trends in the frequency of occurrence of sea-state types #3, #7 and #9. The results indicate that at least a joint decadal increase of 2% in sea-state type #3 and a corresponding decrease of 2% in #9 would be needed to generate a small but significant increase for T02pow of 0.05 kW/decade. This would be associated with an overall positive trend of *WEF* of 0.321 kW/m per decade. Such a sharp increase in *WEF* can only be found in the central area of the Bay of Biscay (Fig. 3) and would represent a growing trend more than twice as strong as that observed near Mutriku.

As stated in the first section of this paper, the focus of our study was to identify the number of sea-state types needed to reproduce the

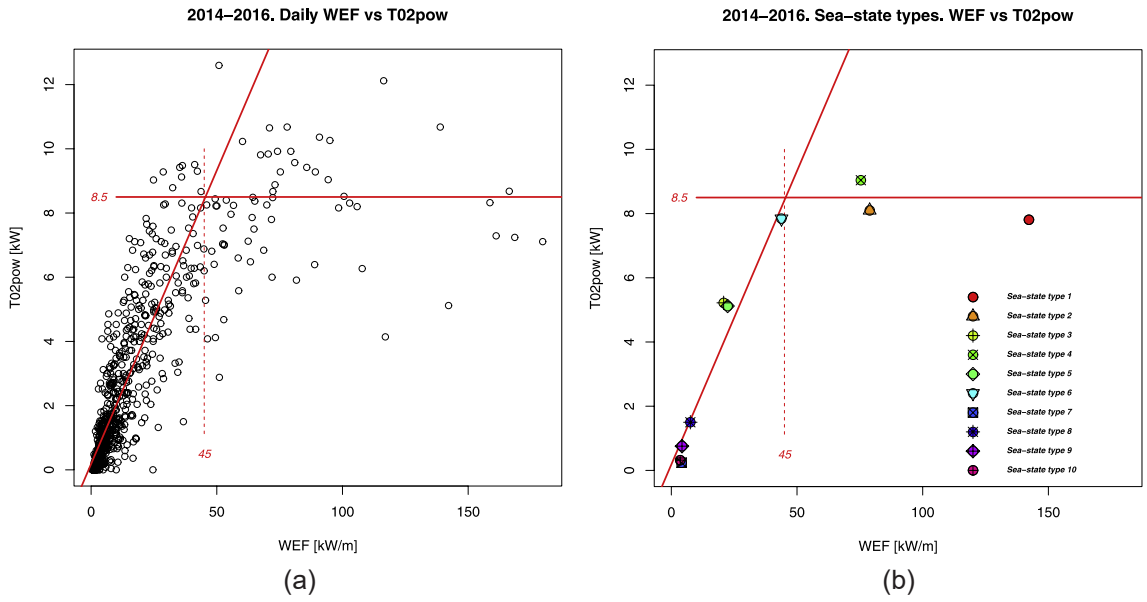

Fig. 4. Training period (2014–2016). *WEF* at point (−2.5° E, 43.5° N) vs T02pow at a daily scale. a) Daily values. b) Sea-state types.

observed electric power generated at Mutriku, rather than to classify waves into clusters with a purely oceanic significance. According to this approach, the profile of the ten sea-state types for the 1979–2019 period remained constant and the increasing energy flux observed in the waves near Mutriku can be attributed to minor, albeit significant, changes in the frequency of occurrence of some sea-state types. The result is a small positive *WEF* trend, mainly affecting its meridional component and resulting in a northward reorientation of the incoming direction. The reasons for this increase are beyond the scope of this work, but some complementary results such as the steady or even declining trends detected for wind speed in many areas of the Bay of Biscay (see Appendix D) suggest that the growing *WEF* trend observed may be due to an increase in the swell component of waves. A recent study for the North Atlantic has used satellite data to confirm the absence of

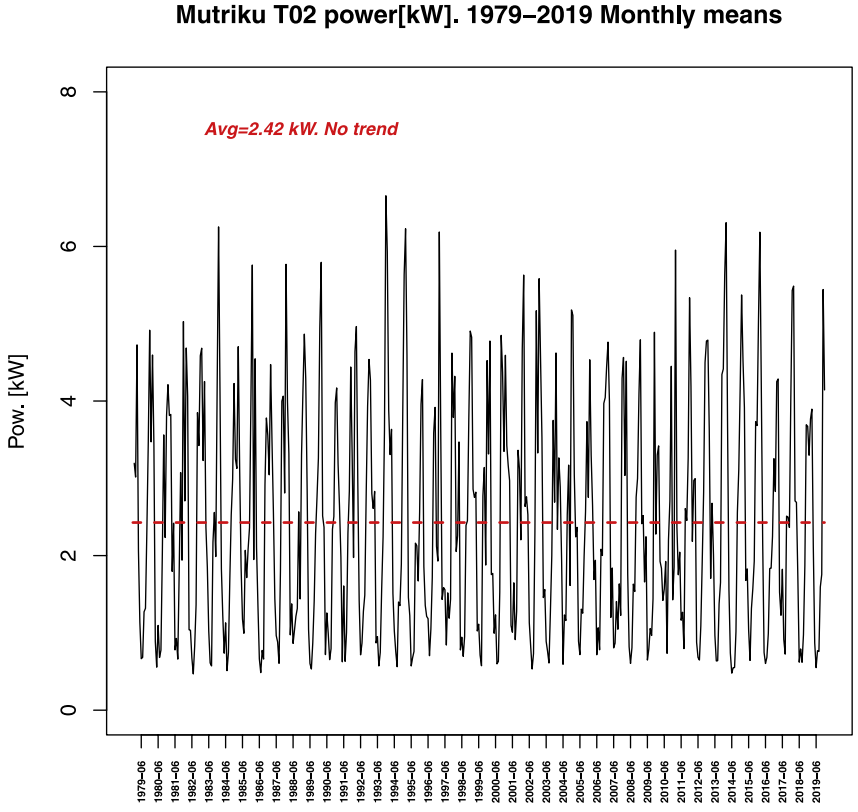

Fig. 5. T02pow monthly averages for period 1979–2019.

significant changes in wind speed trends in this area (Young and Ribal, 2019).

Besides, it is to be noted atmospheric data shows significant amounts of variability at different time scales beyond the ones corresponding to the obvious regular cycles (daily or seasonal). Since waves are driven by wind, these atmospheric oscillations also have an impact on ocean waves. In extratropical regions such as the one covered in this paper, it is known that some of this variability is associated to the development and decay of synoptic perturbations although variability at longer time scales still exists (Blackmon, 1976). The variability associated to time-scales longer than 10 days is commonly referred to as tele-connection patterns, since it is usually apparent in robust correlations between points located far away in the Northern Hemisphere (Wallace and Gutzler, 1981). These results have been corroborated by means of Rotated Principal Component Analysis (Barnston and Livezey, 1987), which is the technique currently commonly used to identify the tele-connection indices over the Northern Hemisphere. Among the Northern Hemisphere teleconnection patterns, is to be mentioned the North Atlantic Oscillation (NAO) which is known to affect synoptic activity over the study area (Rogers, 1997) and is one of the major drivers of climate variations over the European sector (Hurrell, 1995; Hurrel and Van Loon, 1997). A second teleconnection pattern also relevant for this study is the East Atlantic (EA) index, an important player in the area. The EA affects the intensity of advections of southern origin over the area, acting according to a different mechanism of action if compared with the NAO (Sáenz et al., 2001). The wave changes observed in the previous studies commented above on the Bay of Biscay (Le Cozannet et al., 2011; Abadie et al., 2006; Butel et al., 2002; Charles et al., 2012) seem to be driven by changes precisely in the NAO and EA indexes and are reported to concentrate on the swell component. A more general study for the whole Northern Hemisphere has also pointed out the relevance that NAO and EA indexes have at explaining the long-term changes in wave energy (Reguero et al., 2015). In the same study, au-thors also suggest that these trends are far less important for coastal wave farms than those driven by annual seasonality. This statement is particularly relevant for Mutriku, where the strong seasonal pattern observed means that electric power generation in winter is roughly four times higher than in summer (Ibarra-Berastegi et al., 2018) (Fig. 2(b)). If analysed at a monthly scale, the oscillations are even more intense, reaching a proportion of 1–10 between the maximum and minimum values (Fig. 5).

As a conclusion, despite some minor differences, our results above on the evolution of waves are in agreement with those previous studies for the Bay of Biscay carried out using other classification methods and applied to different databases, periods, areas and physical models.

No significant trend was detected in the electric power generated in the second turbine at Mutriku, whereby it may be concluded that the overall electricity generated at Mutriku wave farm would also have remained constant during the 1979–2019 period, if the same set of control, operational and management protocols had been applied. However, these protocols may vary over the years and furthermore, Mutriku occasionally acts as a test facility for different types of wave energy converters that need to be trialled under real operating conditions (Faÿ et al., 2020a; Faÿ et al., 2020b; Rusu and Onea, 2016). A prior paper (Ibarra-Berastegi et al., 2018) has shown that an an average of 10 Wells turbines were working under the regulation and maintenance protocols in place over the 2014–2016 period without any additional device being tested. For these conditions, the annual average electricity sold to the grid was 246468.7 kWh. Under similar steady conditions, the wave farm would have generated a total amount of 10.1 GWh over the 41 years of the 1979–2019 period.

Assuming an average emission factor for the Spanish electric mix of 0.3 kg of CO_2/kWh (European environment agency, 2018; Carbon footprint ltd, 2019; IDAE, 2011; Ministry for ecological transition, 2020) if the Mutriku wave farm had been working since 1979, the emission of 3032 tons of CO_2 would have been avoided. Mutriku is the only wave farm continuously generating electricity, and may also continue contributing in the future to a reduction in greenhouse gas emissions. The Technology Readiness Level (TRL) is an indicator ranging from 1 to 9 to indicate how mature a technological development is (Heder, 2017). 1 corresponds to a basic or initial level while 9 represents a fully commercial and operational level. It is important to mention that although wave energy is at a TRL stage of 7, Mutriku is the only facility that has already reached a TRL of 8 (Strategic research and innovation agenda for ocean energy, 2020). A deeper understanding of the impact of long-term changes in a fully operational wave farm may therefore help in selecting locations (Rusu and Onea, 2013, 2019a, 2019b; Rusu and Guedes Soares, 2012) for different WECs in a dynamic context of constantly evolving wave climate.

5. Conclusions and future outlook

Mutriku is the only wave farm in the world continuously generating electricity since 2011. ERA5 data reveal a generally positive trend in the Bay of Biscay's wave climate over the 1979–2019 period. Operational data from Mutriku were used to fit an optimal SOM and classify obser-vational wave data into ten major sea-state types defined on a daily scale. These types were defined from an energy-generation perspective and not from a purely oceanic point of view. This allowed reconstructing the hypothetical electric power that would have been generated by the Mutriku wave farm, had it been operational over the entire 1979–2019 period. Although the wave climate presents an increasing trend in wave power, the results indicate that this trend would not have meant an increase in electricity production be-cause Mutriku's OWC turbines dampen the effect of the observed positive trends in wave energy. It may therefore be concluded that moderate long-term changes in wave energy may not have a direct impact on the electricity generated at OWC wave farms. It may be inferred that, in the context of climate change, eco-nomic and feasibility studies for prospective wave farms can be con-ducted with a high degree of reliability as future uncertainties in the resource itself are not to have a significant impact on the electric yield during the facility's life cycle.

A new Climate Change law is set to be enacted in Spain in the coming months and 70% of the power generated in the country is expected to be renewable by 2030. Similarly, the European Green Deal (2020) provides a roadmap with actions to cut greenhouse gas emissions and reach a climate neutral EU by 2050. Renewable energies will therefore play an important role although the optimistic projections for wave energy made only a few years ago (Magagna and Uihlein, 2015; OECD, 2016) have now been moderated (Zappa et al., 2019). Within the context of these general plans towards a greener economy, and after nine years operat-ing safely, a wave farm like Mutriku is a facility that can provide a regular and predictable horizon of electricity production.

The authors are currently conducting further research to estimate future wave climate trends in the Bay of Biscay. CMIP5 wave projections using the SAW model have recently been released by the ECMWF (Copernicus cmip5 dataset, 2020) for the RCP4.5 and RCP8.5 scenarios. CSIRO (Commonwealth scientific a, 2020) has also published 21st century wave projections for the same scenarios derived from 10 CMIP5 models (Morim et al., 2020; Csiro cmip5, 2020). Likewise, CMIP6 projections are likely to have been fully disclosed by the end of 2021. These projections will provide estimations of the future wave climate in the Bay of Biscay which will be used to feed the SOM obtained here and obtain estimations of future electricity generation at Mutriku. These results can help to better define the role that wave farms and, particularly, OWC technology can play in meeting the objective of a climate neutral energy generation system.

CRediT authorship contribution statement

Gabriel Ibarra-Berastegi: Conceptualization, Methodology, Writing - original draft, Writing - review & editing. **Alain Ulazia:** Writing - original draft. **Jon Sáenz:** Writing - original draft, Software, Validation. **Paula Serras:** Data curation, Software, Writing - original draft, Supervision. **Santos J. González Rojí:** Data curation, Software, Visualization, Investigation. **Ganix Esnaola:** Software, Validation. **Gregorio Iglesias:** Conceptualization, Methodology, Writing - review & editing.

Declaration of competing interest

The authors declare that they have no known competing financial interests or personal relationships that could have appeared to influence the work reported in this paper.

Acknowledgments

This work has been financially supported by the Spanish Government through the MINECO project CGL2016-76561-R (MINECO/ERDF, UE) and the University of the Basque Country (UPV/EHU, GIU 17/002). ERA5 data have been downloaded at no cost from the Copernicus Climate Data Store. The authors want to express their gratitude to the Basque Energy Agency for kindly providing with operational records from Mutriku wave farm. All the calculations and plots have been carried out in the framework of R (R Core Team, 2020; Wehrens and Kruisselbrink, 2018; Komsta, 2019).

Abbreviations

The following abbreviations are used in this manuscript

CMIP	Coupled Model Intercomparison Project
CSIRO	Commonwealth Scientific and Industrial Research Organization
EA	East Atlantic pattern
ECMWF	European Centre for Medium Range Weather Forecast
H_s	Significant wave height (m)
NAO	North Atlantic Oscillation
m_{wd}	Mean wave direction of the incoming waves. Degrees clockwise from North(°)
T02	Turbine #2 at Mutriku wave farm
T02pow	Daily average of electric power generated by turbine#2 at Mutriku wave farm (kW)
T_m	Mean energy wave period (s)
T_p	Peak wave period (s)
WS	Wind speed (m/s)
WEF	Wave energy flux (kW/m)
WEF_u	Zonal component of the wave energy flux (kW/m)
WEF_v	Meridional component of the wave energy flux (kW/m)

APPENDIX A. 2 × 5 SOM

The candidate SOMs tested in this paper were fitted in unsupervised mode and finally selected under the condition that the observed electric power generated in the test dataset could be succesfully reproduced. In the absence of previous examples of SOM applications for similar purposes, a classical approach (Kohonen, 1982, 1991) was implemented to fit the appropriate SOM leading to the identification and characterization of the optimum number of sea-states. However, it is to be noted that although not necessary for our study, further developments in the implementation of Self-Organizing Maps like the two-steps SOM (TSOM) may be needed in the future to address more complex challenges like the identification of wave extremes (Barbariol et al., 2016).

Here, each daily sea-state has been defined in an 18-dimension hyperspace constituted by the standardized ERA5 values at the nearest grid point every 4 h corresponding to WEF_u, WEF_v and T_p. That is, on a given day, the hourly values at 00 h-04 h-08 h-12 h-16 h–20 h of the zonal and meridional wave energy flux and the peak wave period constitute an 18-dimensional hyperspace. A particular day's sea-state can be seen as a point in it and the final SOM had a 2X5 architecture. This optimal SOM was fitted after 10,000 iterations starting from random values (see Fig. A1a). As the input variables have different operating ranges and units, they are standardized to mean 0 and standard deviation 1. The fitting process progresses until a minimum value of the average distance is reached, in our case of 0.012. Fig. A1b shows the number of cases belonging to the training database mapped onto the different nodes with the final 2 × 5 SOM.

In a SOM, the neighbour nodes in the layout are the ones expected to be more similar to a given node. In other words, neighbouring units hold cases that in the original hyperspace are expected to be closer to each other than to cases belonging to non-neighbouring nodes. The average distance between each unit and their neighbouring nodes in the 2X5 lattice indicates how different each sea-state type can be from the nearest/most similar types. A graphical representation of this can be seen in Fig. A2a, indicating that the nodes/sea-state types #1, #2 and #3 are the ones with the highest distances, thus reinforcing the notion of representing extreme, highly energetic cases with a low frequency, as shown in Table 1 in the main text.

As mentioned in the paper, the input space has 18 dimensions corresponding to the hourly values at 00 h-04 h-08 h-12 h-16 h–20 h of the zonal and meridional wave energy flux and the peak wave period. After fitting the.

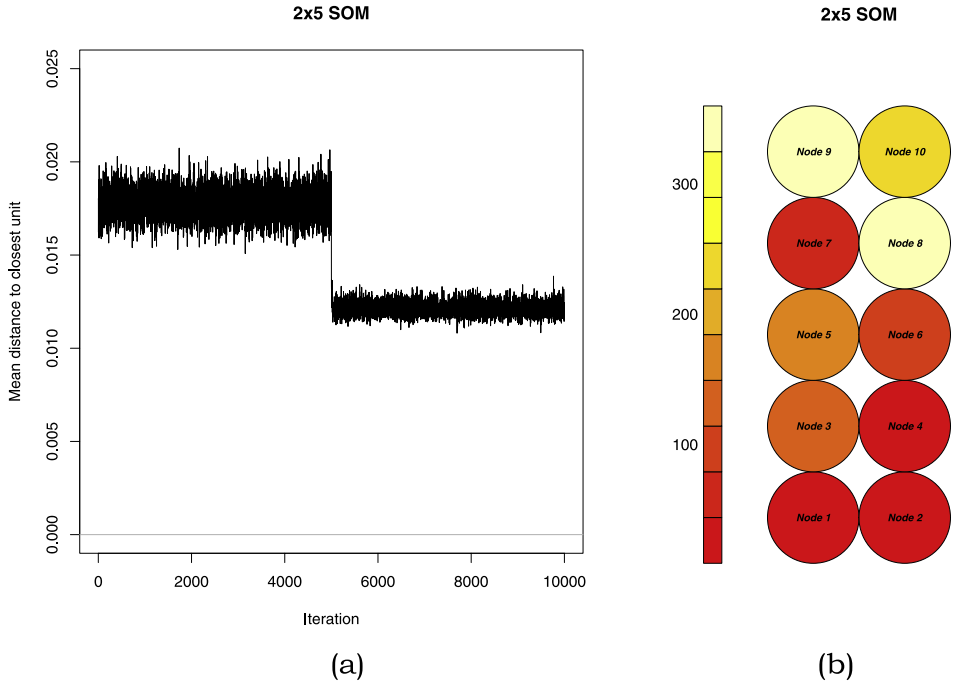

Fig. A1. a) Evolution of the average distance to the closest unit during the fitting process. b) Number of cases mapped onto the 2×5 SOM in the training dataset.

SOM, the centre of gravity of the cases falling on each unit of the SOM (after standardization) are known as *codevectors* and represent the ideal node or in this case sea-state type. Fig. A2b provides a schematic representation of the 18 values corresponding to each codevector for each SOM unit. Once fitted, new cases presented to the SOM will be assigned to the node/sea-state type with the lowest Euclidian distance to its codevector.

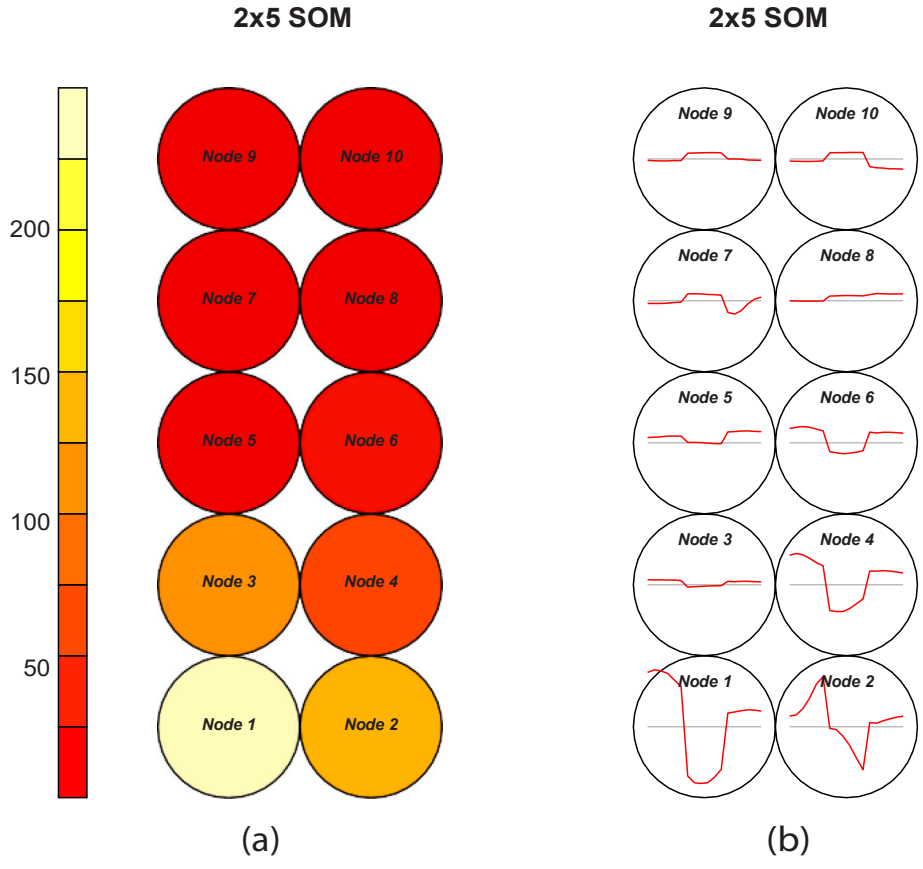

Fig. A2. a) Average distance from each node to its neighbouring units in the 2 × 5 SOM.b) Codevectors for the 2 × 5 SOM.

APPENDIX B. Sea-state types

The information gathered in Table 1 of the paper has been plotted on ten maps of the area -one per node/sea-state type-including directional information of the vectorial variables wave energy flux *WEF* and wind speed *WS* (Figs. B2, B3, B4, B5 and B6). These maps cover the area around the Mutriku wave farm in the Bay of Biscay (Fig B1). Their geographical boundaries are [-3.0° E, −2.0° E] in longitude and [42.8° N, 43.8° N] in latitude. The maps also include information on the frequency of occurrence, distribution by season of the year, H_s, T_m, T_p and T02pow.

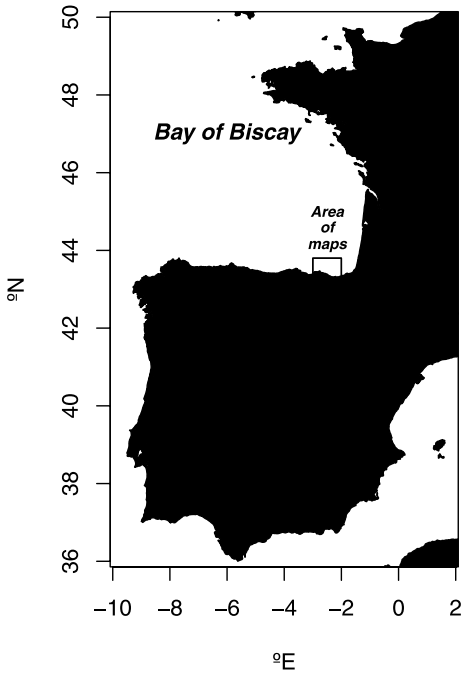

Fig. B1. Bay of Biscay and geographical boundaries of the ten maps.

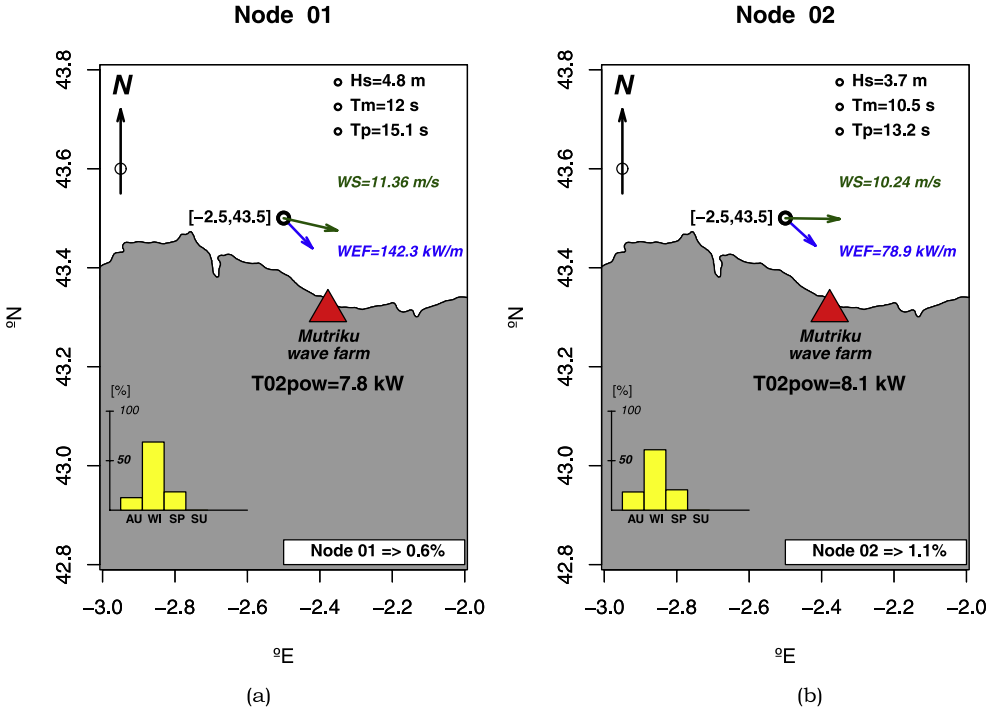

(a) (b)

Fig. B2. a) Node/sea-state type 01. b) Node/sea-state type 02.

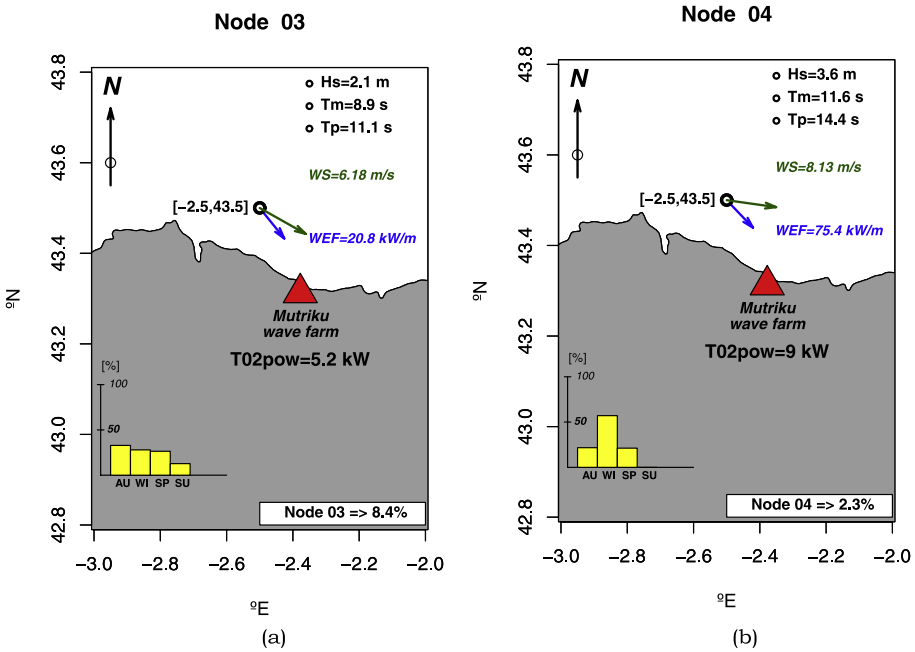

Fig. B3. a) Node/sea-state type 03. b) Node/sea-state type 04.

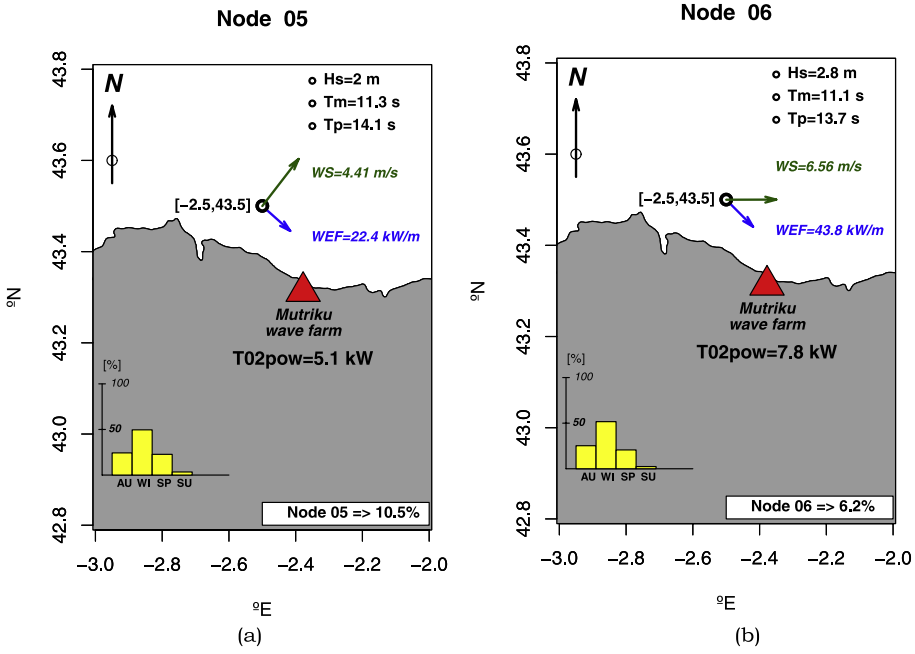

Fig. B4. a) Node/sea-state type 05. b) Node/sea-state type 06.

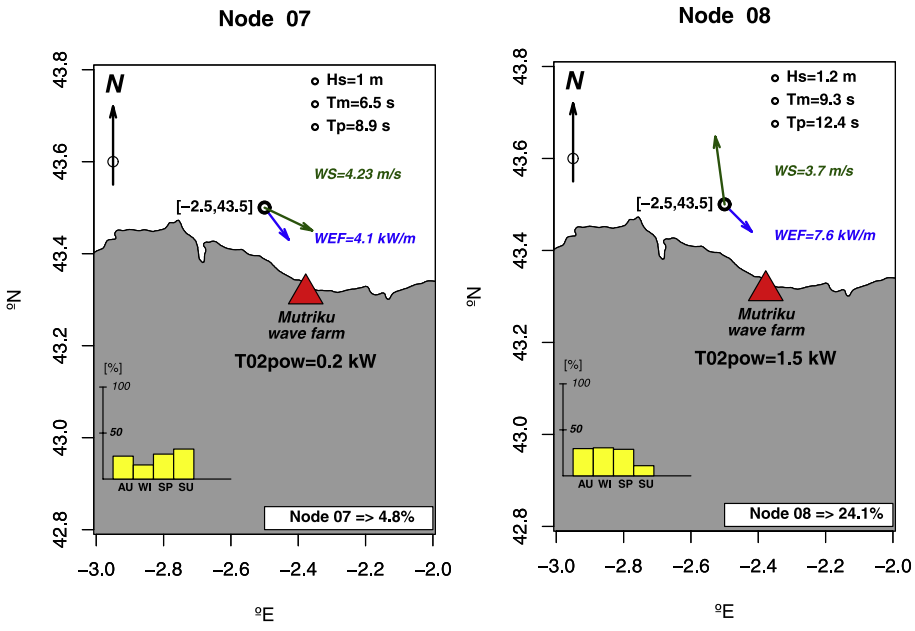

Fig. B5. a) Node/sea-state type 07. b) Node/sea-state type 08.

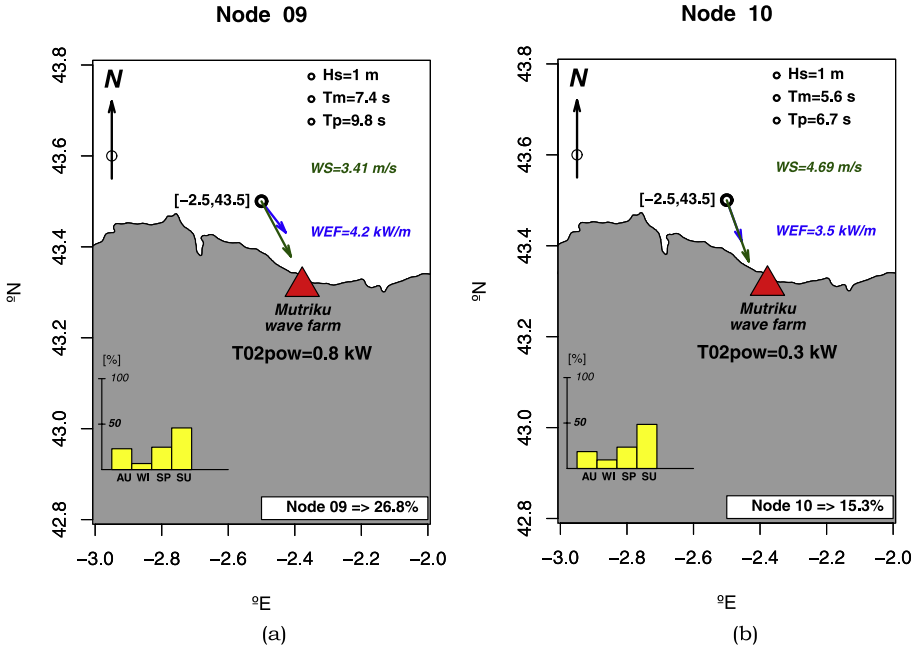

Fig. B6. a) Node/sea-state type 09. b) Node/sea-state type 10.

APPENDIX C. Mutriku Wells turbines

Each of the 14 Wells turbines surmount an air chamber that is part of the breakwater. Incoming waves enter the air chamber below sea level and push an upwards air flow that moves the turbine. As waves withdraw, they generate suction and the air flow is reversed (Fig. C1). Each of the 14 operational turbines includes two Wells-type rotors driving an 18.5 kW generator, rotating in the same direction regardless of the direction of the air flow during the two halves of the cycle (Fig. C2).

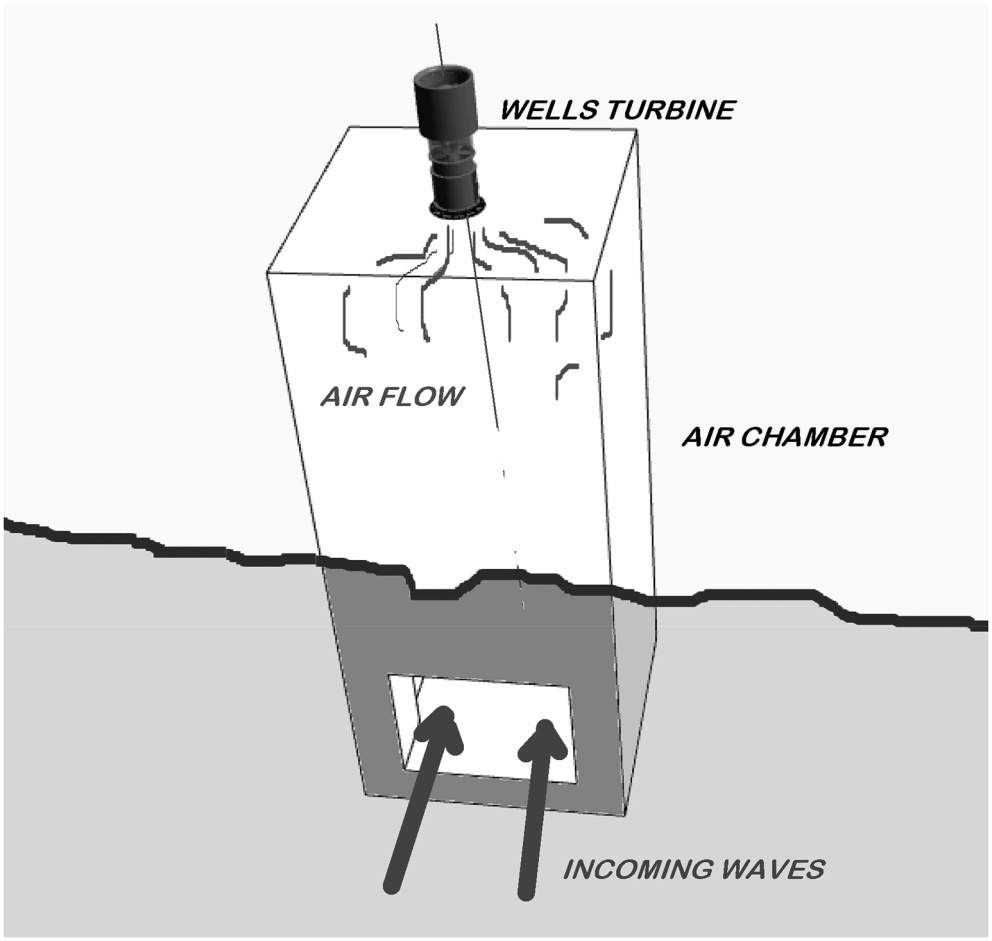

Fig. C1. Layout of one of the air chambers at Mutriku breakwater OWC wave farm.

There is a butterfly valve connecting the air chamber and the Wells device that can be fully open (vertical position, 90°), partially closed or fully closed (horizontal position, 0°).

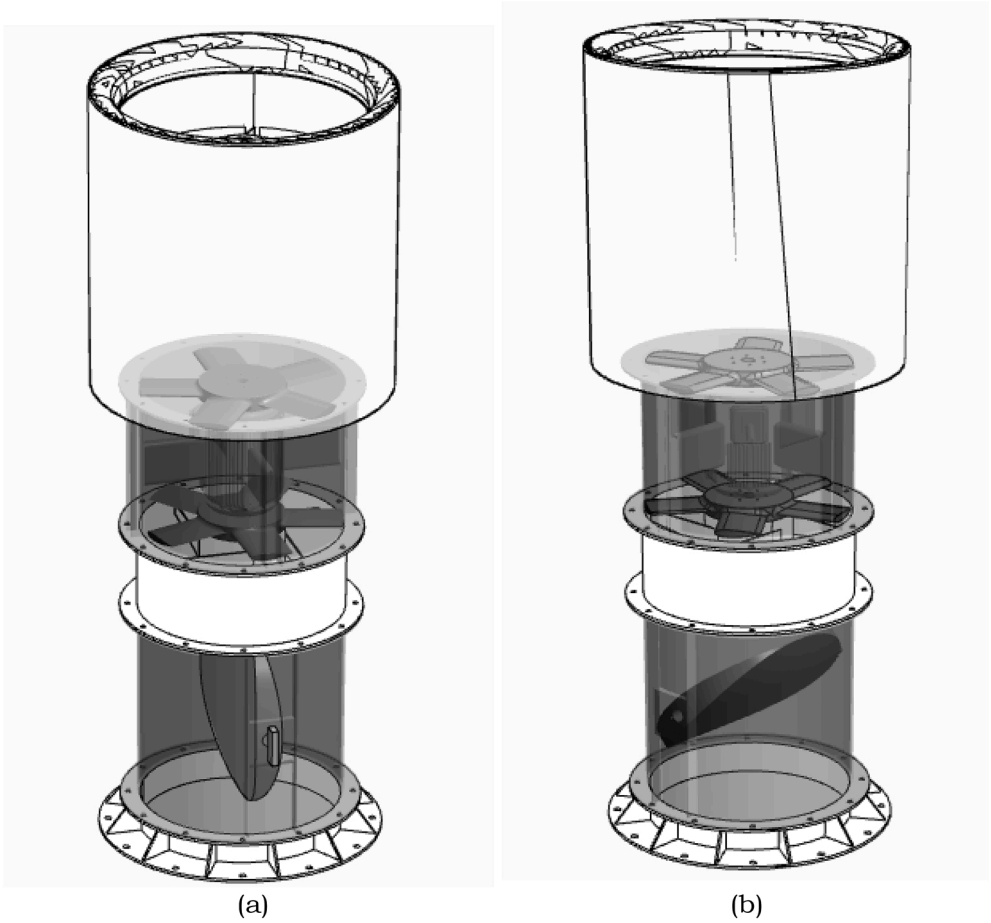

Fig. C2. Wells rotors, generator, connectors and butterfly valve a) Fully open, position 90º, b) Partially open, position 45º.

APPENDIX D. Wind speed trends

Wind speed (*WS*) trends for the period 1979–2019 in the Bay of Biscay have also been calculated (Fig. D1). There are areas near the French coast with negative trends, and some of the areas with the highest positive trends in *WEF* do not have significant trends in *WS*. This suggests that waves generated by local winds can be expected to remain constant and in these areas, the positive *WEF* trends in the Bay of Biscay may be driven by the growing trends of the wave swell component, something already pointed out in previous works on the area (Le Cozannet et al., 2011; Abadie et al., 2006; Butel et al., 2002; Charles et al., 2012). Finally, in the western part of the Bay of Biscay, in latitudes between 44° and 46° N, *WS* records positive trends that may also contribute to the increasing evolution of *WEF* that has been observed.

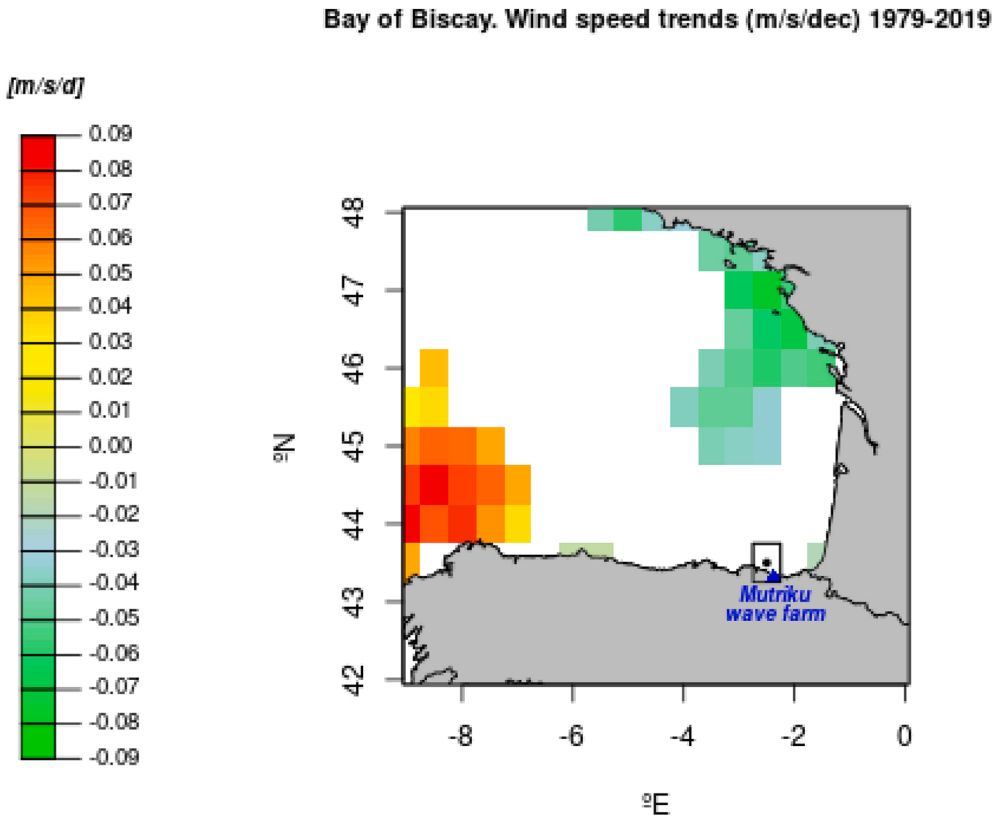

References

Abadie, S., Butel, R., Mauriet, S., Morichon, D., Dupuis, H., 2006. Wave climate and longshore drift on the south aquitaine coast. Continent. Shelf Res. 26 (16), 1924–1939.

Amundarain, M., Alberdi, M., Garrido, A.J., Garrido, I., Maseda, J., 2010. Wave energy plants: control strategies for avoiding the stalling behaviour in the wells turbine. Renew. Energy 35 (12), 2639–2648. http://www.sciencedirect.com/science/article/pii/S096014811000176X.

Amundarain, M., Alberdi, M., Garrido, A., Garrido, I., [de la Sen], M., 2012. Neural control for wave power plant during voltage dips. Elec. Power Syst. Res. 92, 96–105. http://www.sciencedirect.com/science/article/pii/S0378779612001927.

Antonio, F.d.O., 2010. Wave energy utilization: a review of the technologies. Renew. Sustain. Energy Rev. 14 (3), 899–918.

Barbariol, F., Falcieri, F., Scotton, C., Benetazzo, A., Carniel, S., Sclavo, M., 2016. Wave extreme characterization using self-organizing maps. Ocean Sci. 12, 403–415. https://doi.org/10.5194/os-12-403-2016.

Barnston, A.G., Livezey, R.E., 1987. Classification, seasonality and persistence of low-frequency atmospheric circulation patterns. Mon. Weather Rev. 115 (6), 1083–1126.

Basque energy agency, 2020. https://www.eve.eus/?lang=en-gb#. last accesed 2020/August/10.

Bidlot, J.-R., 2020. Ocean Wave Model Output Parameters. https://confluence.ecmwf.int/display/CKB/ECMWF+Model+Documentation?preview=%2F59774192%2F59774191%2Fwave_parameters.pdf. last accesed 2020/August/10.

Biscay Marine Energy Platform-Basque Energy Agency, 2020. https://www.bimep.com/area-mutriku/servicios/. last accesed 2020/August/10.

Blackmon, M.L., 1976. A climatological spectral study of the 500 mb geopotential height of the northern hemisphere. J. Atmos. Sci. 33 (8), 1607–1623.

Butel, R., Dupuis, H., Bonneton, P., 2002. Spatial variability of wave conditions on the French atlantic coast using in-situ data. J. Coast Res. 36 (sp1), 96–108.

Caballero, A., Pascual, A., Dibarboure, G., Espino, M., 2008. Sea level and eddy kinetic energy variability in the Bay of Biscay, inferred from satellite altimeter data. J. Mar. Syst. 72 (1–4), 116–134.

Camus, P., Cofiño, A., Méndez, F., Medina, R., 2011. Multivariate wave climate using self-organizing maps. J. Atmos. Ocean. Technol. 28, 1554–1568. https://doi.org/10.1175/JTECH-D-11-00027.1.

Camus, P., Menéndez, M., Méndez, F.J., Izaguirre, C., Espejo, A., Cánovas, V., Pérez, J., Rueda, A., Losada, I.J., Medina, R., 2014. A weather- type statistical downscaling framework for ocean wave climate. J. Geophys. Res.: Oceans 119 (11), 7389–7405. https://doi.org/10.1002/2014JC010141.

Camus, P., Herrera, S., Gutiérrez, J., Losada, I., 2019. Statistical downscaling of seasonal wave forecasts. Ocean Model. 138, 1–12.

Carbon Footprint Ltd, 2019. https://www.carbonfootprint.com/docs/2019_06_emissions_factors_sources_for_2019_electricity.pdf. last accesed 2020/August/10.

Charles, E., Idier, D., Thiébot, J., Le Cozannet, G., Pedreros, R., Ard- huin, F., Planton, S., 2012. Present wave climate in the bay of biscay: spatiotemporal variability and trends from 1958 to 2001. J. Clim. 25 (6), 2020–2039.

Commonwealth Scientific and Industrial Research Organisation, 2020. https://www.csiro.au. last accesed 2020/August/10.

Copernicus climate data store, 2020. https://cds.climate.copernicus.eu/. last accesed 2020/August/10.

Copernicus Cmip5 Dataset, 2020. https://cds.climate.copernicus.eu/cdsapp#!/dataset/sis-ocean-wave-timeseries?tab=form. last ac- cesed 2020/August/10.

Csiro Cmip5, 2020. https://research.csiro.au/slrwavescoast/waves/cowclip/. last accesed 2020/August/10.

ECMWF, 2020. European Center Medium Range Weather Forecast. https://apps.ecmwf.int/datasets/. last accesed 2020/August/10.

European environment agency, 2018. https://www.eea.europa.eu/data-and-maps/daviz/co2-emission-intensity-5#tab-googlechartid_chart_11_filters=%7B%22rowFilters%22%3A%7B%7D%3B%22columnFilters%22%3A%7B%22pre_config_ugeo%22%3A%5B%22European%20Union%20(current%20composition)%22%3B%22Spain%22%5D%7D%7D. last accesed 2020/August/10.

European Green Deal, 2020. https://ec.europa.eu/info/strategy/priorities-2019-2024/european-green-deal_en. last accesed 2020/August/10.

Ezcurra, A., Sáenz, J., Ibarra-Berastegi, G., Areitio, J., 2008. Rainfall yield characteristics of electrical storm observed in the Spanish Basque country area during the period 1992-1996. Atmos. Res. 89 (3), 233–242.

Fairley, I., Lewis, M., Robertson, B., Hemer, M., Masters, I., Horrillo-Caraballo, J., Karunarathna, H., Reeve, D.E., 2020. A classification system for global wave energy resources based on multivariate clustering. Appl. Energy 262, 114515. http://www.sciencedirect.com/science/article/pii/S0306261920300271.

Faÿ, F.-X., Robles, E., Marcos, M., Aldaiturriaga, E., Camacho, E.F., 2020a. Sea trial results of a predictive algorithm at the mutriku wave power plant and controllers assessment based on a detailed plant model. Renew. Energy 146, 1725–1745.

Faÿ, F.-X., Henriques, J.C., Kelly, J., Mueller, M., Abusara, M., Sheng, W., Marcos, M., 2020b. Comparative assessment of control strategies for the biradial turbine in the mutriku owc plant. Renew. Energy 146, 2766–2784. http://www.sciencedirect.com/science/article/pii/S0960148119312613.

Folley, M., Whittaker, T., Vanâ€™t Hoff, J., 2007. The design of small seabed- mounted bottom-hinged wave energy converters. In: Proceedings of the 7th European Wave and Tidal Energy Conference, vol. 455, p. 312.

Gibson, P.B., Perkins-Kirkpatrick, S.E., Uotila, P., Pepler, A.S., Alexander, L.V., 2017. On the use of self-organizing maps for studying climate extremes. J. Geophys. Res.: Atmospheres 122 (7), 3891–3903.
González, M., Fontán, A., Esnaola, G., Collins, M., 2013. Abrupt changes, multidecadal variability and long-term trends in sea surface temperature and sea level datasets within the southeastern bay of biscay. J. Mar. Syst. 109, S144–S152.
Heder, M., 2017. From NASA to EU: the evolution of the TRL scale in public sector innovation. Innovat. J. 22 (2), 1–23.
Hersbach, H., 2016. The era5 atmospheric reanalysis. In: AGU Fall Meeting Abstracts, p. 12.
Hurrel, J.W., Van Loon, H., 1997. Decadal variations in climate associated with the NAO. Clim. Change 36, 301–326.
Hurrell, J.W., 1995. Decadal trends in the north atlantic oscillation: regional temperatures and precipitation. Science 269 (5224), 676–679.
Ibarra-Berastegi, G., Sáenz, J., Ezcurra, A., Ganzedo, U., de Argandoña, J.D., Errasti, I., Fernandez-Ferrero, A., Polanco-Martínez, J., 2009. Assessing spatial variability of SO2 field as detected by an air quality network using self-organizing maps, cluster, and principal component analysis. Atmos. Environ. 43 (25), 3829–3836.
Ibarra-Berastegi, G., Sáenz, J., Esnaola, G., Ezcurra, A., Ulazia, A., 2015. Short- term forecasting of the wave energy flux: analogues, random forests, and physics-based models. Ocean Eng. 104, 530–539.
Ibarra-Berastegi, G., Sáenz, J., Esnaola, G., Ezcurra, A., Ulazia, A., Rojo, N., Gallastegui, G., 2016. Wave energy forecasting at three coastal buoys in the Bay of Biscay. IEEE J. Ocean. Eng. 41 (4), 923–929.
Ibarra-Berastegi, G., Sáenz, J., Ulazia, A., Serras, P., Esnaola, G., Garcia-Soto, C., 2018. Electricity production, capacity factor, and plant efficiency index at the Mutriku wave farm (2014-2016). Ocean Eng. 147, 20–29.
IDAE, 2011. https://www.idae.es/uploads/documentos/documentos_Factores_de_Conversion_Energia_y_CO2_(2010)_931cce1e.pdf. last accesed 2020/August/10.
Iglesias, G., Carballo, R., 2010. Wave energy and nearshore hot spots: the case of the se bay of biscay. Renew. Energy 35 (11), 2490–2500.
Kohonen, T., 1982. Self-organized formation of topologically correct feature maps. Biol. Cybern. 43 (1), 59–69.
Kohonen, T., 1991. Self-organizing maps: optimization approaches. In: Arti- Ficial Neural Networks. Elsevier, pp. 981–990.
Kohonen, T., 1997. Exploration of very large databases by self-organizing maps. In: Proceedings of International Conference on Neural Networks (Icnnâ€™97), vol. 1. IEEE, pp. PL1–PL6.
Kohonen, T., Somervuo, P., 2002. How to make large self-organizing maps for nonvectorial data. Neural Network. 15 (8–9), 945–952.
Komsta, L., 2019. Mblm: Median-Based Linear Models, R Package Version 0.12.1. URL. https://CRAN.R-project.org/package=mblm.
Kulp, S.A., Strauss, B.H., 2019. New elevation data triple estimates of global vulnerability to sea-level rise and coastal flooding. Nat. Commun. 10 (1), 1–12.
Le Cozannet, G., Lecacheux, S., Delvallee, E., Desramaut, N., Oliveros, C., Pedreros, R., 2011. Teleconnection pattern influence on sea-wave climate in the bay of biscay. J. Clim. 24 (3), 641–652.
Lekube, J., Garrido, A.J., Garrido, I., Otaola, E., Maseda, J., 2018a. Flow control in wells turbines for harnessing maximum wave power. Sensors 18 (2), 535.
Lekube, J., Garrido, A.J., Garrido, I., Otaola, E., 2018b. Output power improvement in oscillating water column-based wave power plants. Rev. Iberoam. Autom. Inf. Ind. 15 (2), 145–155.
Liu, Y., Weisberg, R.H., Mooers, C.N., 2006. Performance evaluation of the self-organizing map for feature extraction. J. Geophys. Res.: Oceans 111 (C5).
López, I., Pereiras, B., Castro, F., Iglesias, G., 2016. Holistic performance analysis and turbine-induced damping for an owc wave energy converter. Renew. Energy 85, 1155–1163.
Magagna, D., Uihlein, A., 2015. Ocean energy development in eu- rope: current status and future perspectives. Int. J. Mar. Energy 11, 84–104. http://www.sciencedirect.com/science/article/pii/S2214166915000181.
Ministry for ecological transition, 2020. https://www.miteco.gob.es/en/cambio-climatico/temas/mitigacion-politicas-y-medidas/calculadoras.aspx. last accesed 2020/August/10.
Morim, J., Trenham, C., Hemer, M., Wang, X.L., Mori, N., Casas- Prat, M., Semedo, A., Shimura, T., Timmermans, B., Camus, P., et al., 2020. A global ensemble of ocean wave climate projections from cmip5-driven models. Sci. Data 7 (1), 1–10.
Multon, B., 2013. Marine Renewable Energy Handbook. John Wiley & Sons.
Oecd, 2016. The Ocean Economy in 2030. OECD.
O'Hagan, A., Huertas, C., O'Callaghan, J., Greaves, D., 2016. Wave energy in europe: views on experiences and progress to date. Int. J. Mar. Energy 14, 180–197.
Pereiras, B., López, I., Castro, F., Iglesias, G., 2015. Non-dimensional analysis for matching an impulse turbine to an owc (oscillating water column) with an optimum energy transfer. Energy 87, 481–489.
Perez, J., Menendez, M., Camus, P., Mendez, F.J., Losada, I.J., 2015. Statistical multi-model climate projections of surface ocean waves in europe. Ocean Model. 96, 161–170.
Pérez-Collazo, C., Greaves, D., Iglesias, G., 2015. A review of combined wave and offshore wind energy. Renew. Sustain. Energy Rev. 42, 141–153.
R Core Team, R., 2020. A Language and Environment for Statistical Comput- Ing. R Foundation for Statistical Computing, Vienna, Austria. URL. https://www.R-project.org/.
Reguero, B., Losada, I., Méndez, F., 2015. A global wave power resource and its seasonal, interannual and long-term variability. Appl. Energy 148, 366–380.
Reikard, G., Robertson, B., Bidlot, J.-R., 2015. Combining wave energy with wind and solar: short-term forecasting. Renew. Energy 81, 442–456.
Rogers, J.C., 1997. North atlantic storm track variability and its association to the north atlantic oscillation and climate variability of northern europe. J. Clim. 10 (7), 1635–1647.
Rusu, E., Guedes Soares, C., 2012. Wave energy pattern around the madeira islands. Energy 45 (1), 771–785 the 24th In- ternational Conference on Efficiency, Cost, Optimization, Sim- ulation and Environmental Impact of Energy, ECOS 2011. http://www.sciencedirect.com/science/article/pii/S0360544212005439.
Rusu, E., Onea, F., 2013. Evaluation of the wind and wave energy along the caspian sea. Energy 50, 1–14. http://www.sciencedirect.com/science/article/pii/S0360544212009085.
Rusu, E., Onea, F., 2016. Estimation of the wave energy conversion efficiency in the atlantic ocean close to the european islands. Renew. Energy 85, 687–703. https://doi.org/10.1016/j.renene.2015. 07.042.
Rusu, E., Onea, F., 2019a. An assessment of the wind and wave power potential in the island environment. Energy 175, 830–846. http://www.sciencedirect.com/science/article/pii/S0360544219305468.
Rusu, E., Onea, F., 2019b. A parallel evaluation of the wind and wave energy resources along the Latin american and european coastal environments. Renew. Energy 143, 1594–1607. http://www.sciencedirect.com/science/article/pii/S0960148119307906.
Sáenz, J., Rodríguez-Puebla, C., Fernández, J., Zubillaga, J., 2001. Interpretation of interannual winter temperature variations over southwestern eu- rope. J. Geophys. Res.: Atmospheres 106 (D18), 20641–20651.
Sen, P.K., 1968. Estimates of the regression coefficient based on kendallâ€™s tau. J. Am. Stat. Assoc. 63 (324), 1379–1389.
Serras, P., Ibarra-Berastegi, G., Sáenz, J., Ulazia, A., 2019. Combining random forests and physics-based models to forecast the electricity generated by ocean waves: a case study of the mutriku wave farm. Ocean Eng. 189, 106314.
Siegel, A.F., 1982. Robust regression using repeated medians. Biometrika 69 (1), 242–244.
Strategic Research and Innovation Agendafor Ocean Energy, 2020. https://www.ocean-energy-europe.eu/wp-content/uploads/2020/05/ETIP-Ocean-SRIA.pdf. last accesed 2020/August/10.
Theil, H., 1950. A rank-invariant method of linear and polynominal regression analysis (parts 1-3). Ned. Akad. Wetensch. Proc. Ser. A 53, 1397–1412.
Torre-Enciso, Y., Ortubia, I., De Aguileta, L.L., Marqués, J., 2009. Mutriku wave power plant: from the thinking out to the reality. In: Proceedings of the 8th European Wave and Tidal Energy Conference, vol. 710, pp. 319–329. Uppsala, Sweden.
Ulazia, A., Penalba, M., Ibarra-Berastegui, G., Ringwood, J., Sáenz, J., 2017. Wave energy trends over the bay of biscay and the consequences for wave energy converters. Energy 141, 624–634.
Ulazia, A., Penalba, M., Ibarra-Berastegui, G., Ringwood, J., Sáenz, J., 2019. Reduction of the capture width of wave energy converters due to long- term seasonal wave energy trends. Renew. Sustain. Energy Rev. 113, 109267.
Vilibic, I., Sepic, J., Mihanovic, H., Kalinic, H., Cosoli, S., Janekovic, I., Zagar, N., Jesenko, B., Tudor, M., Dadic, V., et al., 2016. Self-organizing maps- based ocean currents forecasting system. Sci. Rep. 6, 22924.
Wallace, J.M., Gutzler, D.S., 1981. Teleconnections in the geopotential height field during the northern hemisphere winter. Mon. Weather Rev. 109 (4), 784–812.
Wehrens, R., Kruisselbrink, J., 2018. Flexible self-organizing maps in kohonen 3.0. J. Stat. Softw. Artic. 87 (7), 1–18. URL. https://www.jstatsoft.org/v087/i07.
Wehrens, R., Buydens, L.M., et al., 2007. Self-and super-organizing maps in r: the kohonen package. J. Stat. Software 21 (5), 1–19.
Young, I.R., Ribal, A., 2019. Multiplatform evaluation of global trends in wind speed and wave height. Science 364 (6440), 548–552.
Zappa, W., Junginger, M., [van den Broek], M., 2019. Is a 100% renewable european power system feasible by 2050? Appl. Energy 233–234, 1027–1050. https://doi.org/10.1016/j.apenergy.2018.08. 109.
Zheng, S., Antonini, A., Zhang, Y., Greaves, D., Miles, J., Iglesias, G., 2019. Wave power extraction from multiple oscillating water columns along a straight coast. J. Fluid Mech. 878, 445–480. https://doi.org/10.1017/jfm.2019.656.
Zheng, S., Zhu, G., Simmonds, D., Greaves, D., Iglesias, G., 2020a. Wave power extraction from a tubular structure integrated oscillating water column. Renew. Energy 150, 342–355. http://www.sciencedirect.com/science/article/pii/S0960148120300094.
Zheng, S., Antonini, A., Zhang, Y., Miles, J., Greaves, D., Zhu, G., Iglesias, G., 2020b. Hydrodynamic performance of a multi-oscillating water column (owc) platform. Appl. Ocean Res. 99, 102168. http://www.sciencedirect.com/science/article/pii/S014111871931123X.